For submission to **BBA** (Special Issue on Transferrin) *BBAGEN_11_247_Revised*

Fibrillation of Transferrin

Claire Booyjzsen[a], Charlotte A. Scarff[b], Ben Moreton[a], Ian Portman[b], James H. Scrivens[b], Giovanni Costantini[a], Peter J. Sadler[a,*]

[a] *Department of Chemistry, University of Warwick, Coventry, CV4 7AL, UK.*

[b] *School of Life Sciences, University of Warwick, Coventry, CV4 7AL, UK.*

Keywords

Transferrin; Fibrils; Atomic force microscopy; Transmission electron microscopy; Ion mobility-Mass spectrometry; Neurological disease

* Corresponding author. Email: P.J.Sadler@warwick.ac.uk; Tel: +44 24 765 23818; Fax: +44 24 765 23819

ABSTRACT

The nature of fibrillar deposits from aqueous solutions of human serum and recombinant human transferrin on mica and carbon-coated formvar surfaces has been investigated. Atomic force microscopy showed that the deposition of recombinant transferrin onto the hydrophilic surface of mica resulted in the formation of a monolayer-thick film composed of conformationally-strained flattened protein molecules. Elongated fibres developed on top of this layer and appeared to be composed of single proteins or small clusters thereof. Monomeric and dimeric transferrin were separated by gel permeation chromatography and their states of aggregation confirmed by mass spectrometry and dynamic light scattering. Transmission electron-microscopy showed that dimeric transferrin, but not

monomeric transferrin, deposited on carbon-coated formvar grids forms rounded (circular) structures *ca.* 250 nm in diameter. Small transferrin fibrils *ca.* 250 nm long appeared to be composed of smaller rounded sub-units. Synchrotron radiation-circular dichroism and, Congo red and thioflavin-T dye-binding experiments suggested that transferrin aggregation in solution does not involve major structural changes to the protein or formation of classical β-sheet amyloid structures. Collisional cross sections determined via ion mobility-mass spectrometry showed little difference between the overall protein shape of *apo*- and *holo*-transferrin in the gas phase. The possibility that transferrin deformation and aggregation are involved in neurological disorders such as Parkinson's and Alzheimer's disease is discussed.

Research highlights

→ The association of transferrin dimers is detected by gel permeation chromatography, mass spectrometry and higher order aggregates by dynamic light scattering,

→ Collisional cross sections for *apo*- and *holo*-transferrin are determined by ion mobility-mass spectrometry.

→ Atomic force microscopy detects flattened transferrin on mica surfaces with more pronounced aggregation into fibrils in the second layer

→ Fibres formed by dimers on carbon surfaces are characterised by TEM.

→ The possible relationship between transferrin structural changes, aggregation, iron deposition, and certain diseases merits further investigation.

1. Introduction

Transferrin (Tf) is an ~80 kDa iron-transporting glycoprotein found at 35 μM (~2.5 mg/mL) in the blood. The transferrin superfamily includes serum transferrin (hsTf, found predominantly in the blood), lactoferrin (Lf, found in body fluids such as milk, bile and tears), ovotransferrin (OTf, found predominantly in egg white), melanotransferrin (MTf, found on the surface of cells and associated with growth and differentiation) and the bacterial analogue, ferric ion binding protein (FBP) [1]. Sharing 30% sequence homology, double-lobed transferrin is believed to result from a gene duplication of the mono-lobal bacterial homologue [2]. Human transferrin (hTf) is composed of alternating α-helices and β-sheets separated into an N-lobe and a C-lobe, each further sub-divided into domains I and II, **Fig. 1**. A short random coil (hTf) or α-helix (Lf) joins the two lobes. There is one similar Fe(III) binding site in each of the N- and C-lobe inter-domain clefts, consisting of Fe(III) co-ordinated with distorted octahedral geometry by an histidine, two tyrosinates and an aspartate, along with a bidentate synergistic anion, usually carbonate (or bicarbonate) which is essential for strong metal binding [1]. The open cleft can close after metal capture in a manner characteristic of proteins from the "Venus fly-trap" family [1,5,6]. A wide range of other metal ions such as Mn^{3+}, Al^{3+}, Ga^{3+}, Ti^{4+} and Hf^{4+} can also bind to Tf, which is often considered to form part of the body's generic metal transport system [1].

Iron plays a crucial role in the brain, for example in neurotransmitter synthesis, myelin formation and growth [7,8,9]. Transferrin is known to be present in the brain [7-13], where control of iron transport is especially important. The risks associated with iron overload are well documented [10,11] and there is current interest in the role that iron may play in some neurodegenerative diseases [7,8,9]. Abnormalities in iron distribution in the brain may be involved in a variety of neurological disorders. For example, there is now strong evidence that iron transport and regulation play a crucial role in the pathology of

Alzheimer's disease (AD). Iron overload may be a causative factor in the development of AD. An interaction between the transferrin gene (TF) and the haemochromatosis gene (HFE) results in significant association with risk for AD [12,13] and has been linked to the fibril-forming protein Aβ and iron-overload [12].

It is of interest to ask therefore how transferrin might become involved with the abnormal deposition of iron in the brain. The same question might be asked of manganese since transferrin is the major transporter of manganese, a metal which has also been implicated in neurological disorders [14]. Transferrin is a large flexible protein. Besides opening and closing of the metal-binding cleft, which involves entry of carbonate as an essential synergistic anion, and protonation and deprotonation of metal-binding side-chains, N-lobe(C-lobe): Asp60(395); Tyr92(435); Tyr192(528); His253(597), the two lobes which are joined by a small linker peptide can change their relative positions (as is thought to occur on binding to the transferrin receptor) [15]. Other regions within the protein may similarly be able to adopt variable conformations. There are also two flexible biantennary glycan chains in the C-lobe (attached to Asn413 and Asn611). Although the cleft is usually closed when iron is bound to the protein, this might not be the case if a chelating ligand enters the cleft bound to iron or if an (oxo)iron cluster binds. Such open-cleft binding of an oxo-bridged iron cluster is known for bacterial FBP [16], but has yet to be established for serum transferrin.

The connection between protein misfolding, aggregation, and disease is already well-established, specifically as it relates to amyloid formation, and has been shown to be of importance in a number of diseases (proteinopathies) [17-22]. The formation of various types of fibres (fibrils) appears to play a crucial role in amyloid-like protein deposition diseases (the words fibre and fibril are generally used interchangeably). The mechanism of protein fibril diseases is not fully understood. Nor for example is the nature of the fibrillar deposits. It was first thought that amyloid plaques in the brain were causative in the case of Alzheimer's

disease. However, fibrillar deposits may act as a defence mechanism, removing free oligomers thereby potentially preventing damage otherwise caused by oligomers, although this is still a point of debate [23,24]. Lactoferrin, which shares >85% sequence homology with Tf, has been observed in association with amyloid deposits in the brain [25].

Our initial work on the deposition of human serum transferrin on a variety of surfaces suggested that transferrin can readily form fibres [26]. Moreover under some conditions this appeared to be accompanied by the formation of nano-deposits along the length of the fibre of an iron mineral resembling the iron oxo-hydroxo mineral lepidocrocite, γ-Fe(O)(OH) [26]. This is a similar mineral form to that in which iron ordinarily accumulates within the body's iron storage protein ferritin [27,28]. However, it is clear from (largely TEM) studies in our laboratory over the last 3 years, that not all batches of human serum transferrin readily form fibres on surfaces (C. Booyjzsen, A. Mukherjee and P.J. Sadler, unpublished). It seems likely that small perturbations in the structure of transferrin trigger such behaviour. In the present work we have therefore sought to identify the forms of the protein which can form fibrils. We have used atomic force microscopy to study the deposition of transferrin on mica surfaces, and transmission electron microscopy to study deposition on carbon-coated formvar surfaces. In particular we have also investigated protein aggregation by gel permeation chromatography, dynamic light scattering and mass spectrometry, and structural changes by circular dichroism (CD) and travelling wave ion mobility-mass spectrometry (TWIM-MS). The results show that transferrin has a flexible deformable structure. The ability of transferrin to form specific aggregates may be of physiological importance.

2. Materials and Methods

2.1 Proteins

Lyophilised, glycosylated, *apo*- and *holo*- human serum transferrin were purchased from Sigma-Aldrich (See **Supplementary Information [SI] 1.1**); the iron content was confirmed by ICP-MS analysis. Deglycosylated *holo*-human serum transferrin expressed recombinantly (rTf) in *Saccharomyces cerevisiae* was the gift of Novozymes, and was used as received or purified via FPLC and/or dialysis (**SI. 1.1**). All media in which the protein was dissolved were sterilised by autoclaving at 121°C, and protein solutions were passed through a sterile 0.1 μm filter (Millipore, U.K.) into sterile receptacles, either purchased as such or autoclaved at 121°C. Protein solutions were stored at -4°C.

Attention was devoted to the preparation and deposition of transferrin samples under sterile conditions to minimise the possibility of observing microorganisms on the surfaces studied. This included the use of a category-1 laminar flow hood for preparation and handling of all samples.

2.2 Protein purification

Recombinant *holo*-Tf was purified on an Äkta (General Electric, Sweden) fast protein liquid chromatography (FPLC) system, equipped firstly with a HiPrep 26/60 Sephacryl S200 HR gel filtration column (GE Healthcare Biosciences, Sweden) (see **Supplementary Information** section **SI. 1.1; 2.1** and **Fig. SI. 1**) and subsequently, a 5 mL HitrapCapto-Q anion exchange column (Amersham Biosciences, Sweden).

2.3 Reversed phase-liquid chromatography-mass spectrometry^{E}

To confirm the sequence of *holo*-rTf, the protein was subjected to tryptic digestion and then analysed by reversed-phase (RP) liquid chromatography (LC) - MS^{E} (elevated energy) [29]. Protein samples were prepared at a concentration of 200 pmol/μL in 3% acetronitrile and subjected to Rapigest (Millipore, U.K.) digestion prior to analysis [30]. RP-

LC was performed on a Waters Nanoacquity system equipped with a C18 (1.6 µM) column. An aqueous mobile phase of 0.1 % formic acid (HCOOH) was used and an organic mobile phase consisting of acetonitrile (ACN) 0.1 % HCOOH. A Waters Synapt HDMS system was used for mass spectrometric data acquisition. Data were acquired in a data-independent manner by alternating between low and elevated energy scan functions, from which intact precursor and peptide fragmentation information were obtained, respectively [29]. The data were processed and matched against an in-house database including the putative rTf sequence by use of ProteinLynx Global Server v.2.4.

2.3 Atomic force microscopy

Recombinant human *holo*-transferrin was diluted to 1 µM in 1 mM analytical grade ammonium bicarbonate (Fischer Scientific, U.K.). Samples were then desalted and exchanged into 0.2 micron-filtered, double-distilled water using a 10 kDa molecular weight cut-off spin column (Millipore, U.S.A.). From the resulting solution, 6 µL was drop-cast onto freshly cleaved muscovite mica (SPI, grade V1) and allowed to evaporate in a laminar flow hood.

Atomic force microscopy (AFM) images were recorded using a Veeco Multimode V instrument with a Nanoscope V controller operating in tapping-mode. The cantilevers used for imaging were Bruker FMV Si probes (k~2.8 N/m, nominal tip radius 10 – 12 nm). Images were processed using WSxM software [31]. Quantitative structural characteristics were evaluated by averaging data taken from many images for statistical analysis; errors represent the corresponding standard deviations.

2.4 TEM samples

Samples were applied as 6 µL droplets directly from stock solutions onto 200 mesh carbon-coated formvar copper grids (Agar Scientific, U.K.) and dried in air in a laminar flow hood. They were stained with 1% uranyl acetate, to enhance protein contrast. Stain was applied as a 1 – 3 µL droplet then removed by capillary action using filter paper after 30 – 60 s. One water droplet was then applied and removed in the same way to eliminate excess stain. Electron micrographs were recorded on a high resolution JEM-2011 (JEOL, Japan) transmission electron microscope operating at an accelerating voltage of 200 kV.

2.5 Native ESI-MS and TWIM-MS

To investigate possible conformational changes in transferrin upon the removal of Fe^{3+}, both *apo*- and *holo*-recombinant proteins were investigated by means of electrospray ionisation-travelling wave ion mobility-mass spectrometry (ESI-TWIM-MS) (see **SI. 1.4**). Ion mobility MS is a shape-selective technique, based on the time taken for an ion to traverse a mobility cell containing an inert gas under the influence of a weak electric field [32]. In TWIM-MS ions are propelled through a mobility cell containing an inert gas (nitrogen in the present case) under the influence of transient voltage pulses (travelling waves) [33]. The rate of travel depends predominantly on the physical size, charge and shape of gas-phase ions [34]. Ion drift times or arrival time distributions are thus dependent on their collision cross-section (CCS) which can be calculated with reference to a known standard (myoglobin) [35-38]. *Holo*-rTf (*ca.* 20 µM) was exchanged into 200 mM ammonium acetate and samples prepared over a 7.4 – 5.5 pH range, in 0.5 pH unit increments. *Apo*- and *holo*-samples from Sigma were also prepared in 200 mM ammonium acetate at 20 µM concentrations. Samples were further desalted and buffer-exchanged by use of 10 kDa Millipore Ultrafree 0.5 mL centrifugal-filter devices into 200 mM ammonium acetate for native MS analysis. A further sample of recombinant transferrin was denatured in 50 % ACN 0.2% HCOOH.

A Synapt HDMS G2 system (Waters, Manchester, U.K.) was used to perform all ESI-TWIM-MS experiments. Acquisition parameters were optimised to allow for transmission of higher *m/z* ions under near-native conditions. The following instrument conditions were used: backing pressure 8.5 mBar, capillary voltage 1.2 – 1.8 kV, cone voltage 90 V, helium cell gas flow 180 mL/min, IMS cell gas flow 90 mL/min, travelling-wave height 40 V and travelling wave velocity 700 m/s.

Multiply-charged ions of sperm whale myoglobin with known CCS (Ω) values were used to calibrate the data obtained to allow CCS values for transferrin species to be estimated. All mass spectrometry data were processed by use of MassLynx v 4.1 (Waters).The ESI-MS spectrum obtained upon analysis of transferrin prepared in denaturing solvent was deconvoluted onto a true mass scale by use of the MaxEnt algorithm (Waters) to obtain accurate molecular weights for the transferrin species studied.

In order to provide an estimate of the change in CCS which can be expected from the opening of one lobe of Tf, theoretical collision cross-sections for the *apo*-N-lobe (PDB ID 1BTJ) and *holo*-N-lobe (PDB ID 1A8E) of transferrin were estimated from their known crystal structures by use of the open source software program MOBCAL [39,30]. MOBCAL can be used to estimate the theoretical collisional cross-section of any molecule with a 3-D co-ordinate file in three models: the Projection Approximation (PA, typically underestimates), Exact Hard Sphere Scattering (EHSS, typically overestimates) and the Trajectory Method (TM, computer intensive).

2.6 Synchrotron radiation-circular dichroism of recombinant transferrin and dynamic light scattering

Synchrotron radiation-circular dichroism (SR-CD) spectra over the wavelength range 178 – 256 nm were recorded at the Institute for Storage Ring Facilities (ISA), Aarhus University, in Aarhus, Denmark.

Dynamic light scattering (DLS) measurements were recorded on a Malvern Nano-S (Malvern Instruments Ltd., U.K.). Samples of 1 μM *holo*-rTf in 10 mM ammonium bicarbonate were investigated by both techniques.

3. Results and Discussion

Our previous studies [26] showed that human serum transferrin can form fibrils when deposited on a variety of surfaces, and under some conditions can lead to the release of iron and formation of (hydr)oxo iron nanominerals. However subsequent work, using predominantly TEM, has shown that not all batches of serum transferrin exhibit this behaviour (C. Booyjzsen, A. Mukherjee and P.J. Sadler, unpublished). Inter-batch differences such as metal content (A. Mukherjee and P.J. Sadler, unpublished) and glycosylation [26] do not appear to account for this. In the present work we therefore sought to compare hsTf with recombinant human transferrin since the latter is likely to be more homogeneous than hsTf. Moreover we have investigated the state of aggregation of the protein in solution before deposition using gel permeation chromatography, mass spectrometry and dynamic light scattering. We also probed the structure of the protein using ion mobility-mass spectrometry, circular dichroism and dye-binding to detect possible amyloid structures. As well as TEM, we have used AFM to characterise the deposited proteins.

First we carried out MS experiments to determine the composition of rTf. Unlike human serum transferrin which contains 2 biantennary glycan chains attached to Asn413 and Asn611 in the C-lobe, rTf expressed in *Saccharomyces cerevisiae* was not expected to be

glycosylated. Our previous work [26] suggested that deglycosylation does not affect the ability of transferrin to form fibres.

3.1 Sequence analysis of recombinant transferrin by mass spectrometry

The sequence of recombinant human transferrin [6] was confirmed by reversed phase-liquid chromatography MS^E [29] as being that of human transferrin with mutations S415A, N611D, V612P and T613A (**Fig. 2**). These mutations prevent N-linked glycosylation at N413 and N611, but do not change the metal-binding properties. Further analysis by ESI-MS (**Fig. 3**) of transferrin under denaturing solvent conditions confirmed the presence of two transferrin species, fully deglycosylated and another form having a single glycosylation at S32, the only remaining known site of glycosylation present in rTf. The deconvoluted spectrum (**Fig. 3**) indicated two species with masses of 75098 Da and 75260 Da, in agreement with the expected masses of the deglycosylated and singly glycosylated recombinant proteins, respectively.

3.2 AFM of recombinant transferrin

The aggregation of rTf on surfaces was studied by deposition on freshly-cleaved mica, $KAl_2(AlSi_3O_{10})(OH)_2$ [41], a model hydrophilic substrate. After evaporation of the solution, the mica substrate appeared to be covered by a complete layer (inset in **Fig. 4** and **Fig. SI. 2**) composed of rounded features with an average height of 2.5 ± 0.5 nm (**Fig. SI. 3**). This height is less than the dimensions of transferrin observed by x-ray crystallography, *ca.* 9.5 × 6.7 × 6.7 nm [3] (**Fig. 1**), implying that rTf adsorbs on mica as a single layer (see **Supplementary Information** section **SI. 2.2**) but with a structure that is different from that in crystals.

A possible explanation is that both homologous lobes composing the protein interact with the substrate, thereby straining the linker peptide (residues 332–338) and producing an overall flatter conformation. The height of each separate lobe, as determined from the crystal structure, is between 2.5 – 3.5 nm which is comparable with the measured height of the layer. Moreover, it should be taken into account that the interaction with the AFM tip can produce a compression of the proteins, further reducing their measured height. The width of the round features was measured to be 43 ± 7 nm. Reliable information on lateral sizes is more difficult to obtain by means of AFM due to the 'tip-convolution effect' which produces broadening of the true dimensions of investigated objects [42]. However, taking into account the influence of a finite size tip, the width of the observed features corresponds to *ca.* 1-3 transferrin molecules. No long-range periodicity was observed within this layer, although the individual features show a tendency to organise locally in short linear or rounded arrangements composed of *ca.* 5 – 10 units (**Fig. SI. 2**).

A more pronounced aggregation into fibril-like structures was observed on top of the base protein monolayer (**Fig. 4**). We estimate the density of these fibrils to be 10^{-4} μm^2, based on a random AFM mapping of the substrate. The height of the structures in the second layer is 4.9 ± 0.6 nm, more compatible with the size of a single transferrin protein in the crystalline phase (**Fig. 1**). The increase in height of structures, with respect to those observed in the monolayer, may originate from weaker inter-protein interactions compared to the transferrin-mica interaction. This would allow the second-layer proteins to adopt a conformation more analogous to that observed in the crystal.

A width of 53 ± 10 nm was measured consistently both within a single fibre and for different fibres. This is very similar to the lateral size of the features in the first layer and, again taking into consideration the finite size tip, corresponds to 3 ± 2 rTf molecules. The slightly larger value could be due to an increased tip broadening effect for objects that are

isolated instead of closely packed. As can be seen in **Fig. 4**, the fibrils contain an internal structure and appear segmented, the smallest recorded sizes being compatible with those of the rounded features in the first layer. As a consequence, we postulate that fibres are formed by a linear arrangement of the same molecules that compose the primary layer. As discussed above, these could be either single proteins or very small aggregates (*ca.* 2 – 3 units each).

Some fibres appeared to be composed of two sections, one straight and one curved. (**Fig. 4**). The curved part showed approximately the same radius of curvature ~160 nm for all of the measured fibres. At present we do not have a clear explanation for this characteristic curvature, nor for the formation of the fibres themselves. The different assembly behaviour of transferrin molecules which are on top of the base monolayer with respect to those interacting directly with the surface may arise because the former molecules have a different conformation/configuration. This could include a change in the relative orientation of the two lobes of which they are composed [3], or cleft-opening and possibly the loss of iron, but this cannot be established on the basis of the present data alone.

Our initial AFM analyses of transferrin deposited on highly oriented pyrolytic graphite (HOPG) and carbon hydrophobic surfaces suggest that, also in this case, the protein forms structured deposits. Their conformation and formation however, are different to and less reproducible than those observed on mica and require further in-depth study. This may suggest that hydrophobic/philic interactions are important in transferrin fibril formation. The AFM observations suggest therefore that not only is interaction with the surface necessary for fibre formation, but that the specific character of the surface may affect or provide a template for the specific agglomerations observed.

3.3 Native-mass spectrometry analysis of recombinant transferrin

Gel permeation chromatography of *holo*-rTf (**Fig. SI. 1**) gave rise to two peaks which were collected and analysed by ESI-MS. The ESI-MS analysis showed that these corresponded to rTf monomer (**Fig. 5A**) and dimer (**Fig. 5B**). Analysis of the sample indicated the presence of monomer, dimer and also higher-order aggregates.

Within the mass spectrum of recombinant transferrin five main peaks were observed which corresponded to the monomer charge states $[M+17H]^{17+}$ to $[M+21H]^{21+}$. A second distribution at *ca.* m/z 5800 was identified as corresponding to rTf dimer charge states $[M+26H]^{26+}$ to $[M+30H]^{30+}$. GPC fractions corresponding to the first eluted peak contained both monomeric and dimeric rTf suggesting that an equilibrium between the two had been established. MS peaks for the rTf dimer were observable for both *apo*- and *holo*-rTf as well as for commercial Sigma-Aldrich *apo*- and *holo*-hsTf (**Supplementary Information** section **SI. 2.3** and **Fig. SI. 4**). Dimer was detected by ESI-MS in solutions ranging between pH 5.0 and 8.0 (studied in 0.5 increments). Transferrin dimers have not been well studied previously, although their existence has been noted [43-46].

An additional distribution of charge states centred around *ca.* 7200 m/z corresponding to higher order transferrin aggregates, likely either a trimer or tetramer, was also observed (**Fig. 6**). The data, although consistently reproducible, were of insufficient signal strength to allow deconvolution of the spectrum to confirm an accurate mass for these superstructures or gain any meaningful ion mobility data.

3.4 Dynamic light scattering

DLS was carried out to detect the presence of Tf-aggregates in solutions from GPC fractions. DLS of Tf-dimer samples revealed transferrin superstructures. The solution had a polydispersity index (PI or PDI) of 0.707, corresponding to a polydispersity of 84% PD. PD vaues of <20% are often taken to imply the presence of single protein molecules whereas

values > 20% indicate aggregation [47,48] Unchromatographed transferrin and monomeric rTf were too polydisperse to allow measurement of their particle sizes, showing a propensity for ongoing aggregation. DLS measurements are therefore consistent with a tendency towards higher order protein aggregation.

3.5 TEM of monomeric and dimeric recombinant transferrin fractions

The gel permeation chromatography (GPC) fractions of rTf corresponding to transferrin monomer and dimer, previously analysed by ESI-MS, were deposited onto carbon-coated formvar-copper TEM grids, dried in air and imaged using HR-TEM. The initial unchromatographed rTf did not give rise to any distinct deposits on the grid, apart from a small amount of amorphous protein, and in particular no fibrils were observed. Similarly, GPC fractions corresponding to monomeric-rTf displayed only random protein aggregation and no fibrils. Although the possibility that the application of GPC might induce transferrin aggregation cannot be ruled out, the ability of various samples to form fibrils did not appear to correlate with the use of GPC to purify them. This suggests that monomeric transferrin is unable to aggregate and form fibres. Further, it seems that the monomeric fraction may inhibit aggregation when combined with the dimeric fraction, *i.e.* unchromatographed transferrin.

In contrast, dimeric-transferrin fractions gave rounded circular (perhaps spherical) particles, **Fig. 7A-D.** Some amorphous aggregation is evident in the background (**Fig. 7D**) as was seen for the other non-fibril forming fractions. The spheres appeared singly or associated with one another, as is particularly evident in **Fig. 7C**. They varied in size, with an approximate average diameter of 250 nm suggesting the presence of *ca.* 30 Tf-molecules along the diameter.

The dimer GPC fractions also gave rise to other distinctively-shaped deposits on the carbon surface. Straight, rod-like fibres, *ca.* 200 – 250 nm long (suggesting contact of *ca.* 25 Tf-molecules) are shown in **Fig.8A-C**. These fibrils are smaller than those observed previously [26]. A lower amount of randomly-aggregated protein than seen with the other TEM samples is visible in the background of **Fig. 8D**. It is possible that the fibril-like structure in **Fig. 8C** is composed of several smaller, assembled rounded units such as those in the magnified view in **Fig. 7D**. Dynamic light scattering measurements on TEM solution samples showed higher-order protein agglomerations for dimer fractions and a tendency towards aggregation for monomer and whole *holo*-transferrin. Assuming protein close packing and that the particles are approximately ellipsoidal, this would correspond to a total of *ca.* 27 000 Tf molecules. It is not clear why many of the individual rounded-units appear larger than those in the small fibrils. Nor is it clear why the individual circular-deposits have not formed into fibrils or why these fibrils are smaller than those observed previously [26]. It may be that the presence of a particular form of the protein is necessary for continued aggregation.

3.6 Travelling wave ion mobility-mass spectrometry of recombinant transferrin

The effect of Fe^{3+} binding on the shape of transferrin was investigated by TWIM-MS. In this technique the protein travels through a drift tube filled with inert gas where proteins of different size or shape separate according to their mobility through action of a series of transient voltage pulses (travelling waves). Changes in the shape of transferrin might be critical for aggregation and fibre formation.

Extracted arrival time distributions for the $[M+17]^{17+}$ to $[M+19]^{19+}$ charge states of *holo*- and *apo*- rTf were compared. No significant differences were observed. The experimentally-obtained estimated cross-sections for these are shown in **Fig. 9**. The values of

collisional cross sections determined for *apo*-rTf charge states $[M+17]^{17+}$ to $[M+19]^{19+}$ are in broad agreement with the theoretical cross-sections calculated from the crystal structure by use of MOBCAL PA and EHSS approximations. PA and EHSS calculated theoretical values for *apo*-TF (PDB ID 2HAU) were 4143 and 5384 $Å^2$, respectively. The PA approximation is known to underestimate the cross-section of large molecules whilst the EHSS method has been shown to overestimate it. Estimated and experimentally measured cross-sections are in good agreement.

An atomic resolution structure for differic-Tf is not yet available and so theoretical cross-section values for *holo*-Tf could not be calculated. MOBCAL estimations for the rotationally-averaged collision cross-sections of transferrin N-lobe in *apo*- and *holo*- forms (PDB Ids 1BTJ [39] and 1A8E [40] respectively) are similar (**Fig. 10**). This indicates that although a known local structural change (cleft-opening) occurs in the Tf structure upon metal release, this has little significant effect on the global conformation of the N-lobe. No significant differences in overall cross-section of the *apo*-Tf and *holo*-Tf were observed in ion mobility experiments suggesting that this is also true for the whole protein. This observation is consistent with the work of Gumerov and Kaltashov [49].

3.7 Circular dichroism and dye-binding as probes for amyloid-like properties of rTf

We investigated whether transferrin in solution has amyloid-like characteristics. Amyloid fibres are usually visible to the naked eye and as such are able to be characterized using fibre-diffraction [50]. As this is not the case with Tf-fibres, monomer and dimer fractions were analysed by additional techniques commonly used to characterise amyloid fibres, namely circular dichroism and dye-binding [50].

Monomer and dimer GPC fractions were analysed by synchrotron radiation circular dichroism allowing investigation of the far-UV region of the spectrum. This region is

particularly sensitive to changes in the secondary structure of proteins, which allows the detection of extended β-sheet composition, characteristic of amyloid fibres [51,52,53]. The spectra corresponding to the monomeric and dimeric Tf fractions appear very similar (**Fig. 11**). However, there is a slight shift of the bands for the monomer to higher and the dimer to lower wavelengths in the region below 200 nm and vice versa from 200 – 216 nm. This is indicative of a slightly higher β-sheet composition in the dimer fraction, based on the characteristic spectral patterns for proteins of mostly α-helical or mostly β-sheet composition [51,52,53]. SR-CD analysis of transferrin therefore confirms the protein is not substantially amyloid-like in nature. The slightly higher proportion of β-sheet in dimeric-Tf may be related to its observed tendency to aggregate. Dimerisation of transferrin may initiate fibril formation.

The change in absorption and fluorescence of planar aromatic dyes such as the Congo red (CR) and thioflavin T (ThT) are standard tests for the detection of amyloid fibres [54-58]. These dyes intercalate between β-strands. Solutions of Sigma-Aldrich *holo*-transferrin, for which there was EM evidence of fibre formation, were investigated for their dye-binding abilities. These experiments (see **Supporting Information** sections **SI. 1.2; 1.3; 2.4; 2.5** and **Figs. SI. 5; 6**) provided no evidence of amyloid-like behaviour. Therefore we conclude that the formation of transferrin fibrils does not depend substantially on intermolecular interactions of β-sheet motifs in a similar manner to amyloid fibres. However, there are examples of fibril-forming proteins which fail these standard tests, most notably lysozyme [58]. Also interactions with surfaces may perturb the structure of the protein (as is evident from AFM) and so the structures probed in solution may not be those directly relevant to fibre formation.

4. Conclusions

Our previous studies had shown that both *apo*- and *holo*-human transferrin can form fibre-like aggregates on surfaces with morphologies that differ from classical amyloid fibres. Subsequent work in our laboratory (C.Booyjzsen, A.Mukherjee and P.J.Sadler, unpublished) has shown that not all batches of transferrin exhibit this behaviour. The present work suggests that the preformation of transferrin dimers in solution may be a key difference among batches allowing transferrin aggregation and aiding subsequent fibril formation. We therefore probed some of the factors which may be involved.

We have investigated both (commercial) *apo*- and *holo*-human serum transferrin (Sigma-Aldrich) and recombinant human transferrin (Novozymes). The latter was shown by LC-MS^E to consist of nonglycosylated rTf (with the mutations S415A, N611D, V612P, T613A) and also S32 O-linked glycosylated rTf.

Classical amyloid fibres contain a large proportion of β-sheet structure and form in solution. In contrast dye-binding experiments and SR-CD data suggest that solutions of transferrin which form fibres on surfaces do not undergo such structural changes, and that interactions with the surface are likely to play an integral role in fibre formation. Our results suggest that the pre-formation of dimers in solution may predispose Tf towards fibre formation on surfaces. Transferrin oligomers can also be detected by dynamic light scattering and by mass spectrometry. Dimers separated by chromatography and characterised by MS readily formed fibres as seen by TEM, but monomers did not.

Deposition of rTf on mica surfaces appeared to lead to deformation (flattening) of the first layer deposited. Transferrin is a flexible molecule with facile rotation of the two lobes about the connecting peptide, and opening and closing of the inter-domain metal-binding cleft are already well known. The distortion of molecules in this first layer led to the deposition of long, narrow fibrils in the second deposited layer. The next step will be to model such inter-protein contacts, perhaps making use of known crystal packing features

which involve intermolecular contacts between domain edges [3]. It was not possible to determine from the current experiments whether the lobes of some Tf-molecules lose their iron after deposition, or indeed if *apo*-lobes are open or closed, or contain bound carbonate. All these factors could be important for aggregation.

In future work it will be interesting to investigate whether these observations of transferrin aggregation and structural changes on deposition on surfaces are of physiological importance. They may contribute to the aetiology of neurodegenerative diseases that are reported to involve iron deposition in the brain. If so then small molecules that can prevent aggregation might be useful drugs.

Acknowledgements

Some of the equipment used in this research was obtained through Birmingham Science City: 'Innovative Uses for Advanced Materials in the Modern World' with support from Advantage West Midlands and part funded by the European Regional Development Fund. We thank Dr. Arindam Mukherjee; Dr. Lijiang Song; Dr. Ivan Prokes and Mr. Howard Lightfoot for previous work on this project in our laboratory; Professor Vilmos Fulop and Dr. Tiffany Walsh for helpful discussions; Dr. Søren Vrønning Hoffmann and Mr. Daniel Waldron for SR-CD; and Ms. Sue Slade for RP-LCMS. We also thank ERC, BBSRC, The University of Warwick (for CB) and Waters Corporation, for funding, and Drs. Darrell Sleep and Phil Morton of Novozymes for rTf and helpful discussion.

References

1. H.Sun, H.Li, P.J.Sadler, Transferrin as a metal ion mediator, Chem. Rev. 99 (1999) 2817-2842.
2. A.D.Tinoko, C.W.Peterson, B.Lucchese, R.P.Doyle, A.M.Valentine, On the evolutionary significance and metal-binding characteristics of a monolobal transferrin from *Cionaintestinalis,* Proct. Natl. Acad. Sci. 105 (2008) 3268-3273.
3. J.Wally, P.J.Halbrooks, C.Vonrhein, M.A.Rould, S.J.Everse, A.B.Mason, S.K.Buchanan, The crystal structure of iron-free human serum transferrin provides insight into inter-lobe communication and receptor binding, J. Biol. Chem. 281 (2006) 24934-24944.
4. N.Yang, H.Zhang, Q.Hao, H.Sun, PDB crystal structure code 3 QYT of Differic bound human serum transferrin, deposition date 2011/03/03; release date pending.
5. P.Aisen, A.Liebman, Lactoferrin and Transferrin: a comparative study, Biochim. Biophys. Acta 257 (1972) 314-323.
6. R.T.A.MacGillivray, E.Mendez, J.G.Shewale, S.K.Sinah, J.Lineback-Zins, K.Brew, The primary structure of human serum transferrin, J. Biol. Chem. 258 (1983) 3543-3553.
7. J.L.Beard, J.R.Connor, B.C.Jones, Iron in the brain, Nutr. Rev. 51 (1993) 157-170.
8. L.Zecca, M.B.H.Youdim, P.Riederer, J.R.Connor, R.R.Crichton, Iron, brain aging and neurodegenerative disorders, Nat. Rev. Neurosc. 5 (2004) 863-873.
9. J.B.Aquino, P.L.Musolino, M.F.Coronel, M.J.Villar, C.P.Setton-Avruj, Nerve degeneration is prevented by a single intraneural apotransferrin injection into colchicine-injured sciatic nerves in the rat, Brain Res. 1117 (2006) 80-91.
10. C.A.Swanson, Iron intake and regulation: implications for iron deficiency and iron overload, Alcohol 3 (2003), 99-102.

11. K.Schümann, T.Ettle, B.Szegner, B. Elsenhans, N.W.Solomons, Invited review on risks and benefits of iron supplementation recommendations for iron intake revisited, J. Trace Elements Med. Biol. 21 (2007) 147-168.
12. J.S.K.Kauwe, S.Bertelsen, K.Mayo, C.Cruchaga, R.Abraham, P.Hollingworth, D.Harold, M.J.Owen, J.Williams, S.Lovestone, J.C.Morris, A.M.Goate, The Alzheimer's Neuroimaging Initiative, Suggestive synergy between genetic variants in TF and HFE as risk factors for Alzheimer's disease, Am. J. Med. Gen. 153B (2010) 955-959.
13. D.J.Lehmann, M.Schuur, D.R.Warden, N.Hammond, O.Belbin, H.Kölsch, M.G.Lehmann, G.K.Wilcock, K.Brown, P.G.Kehoe, C.M.Morris, R.Barker, E.Coto, V.Alvarez, P.Deloukas, I.Mateo, R.Gwilliam, O.Combarros, A.Arias-Vásquez, Y.S.Aulchenko, M.A.Ikram, M.M.Breteler, C.M.van Duijn, A.Oulhaj, R.Heun, M.Cortina-Borja, K.Morgan, K.Robson, A.D.Smith. Transferrin and HFE genes interact in Alzheimer's disease risk: the Epistasis Project, Neurobiol. Aging. 2010. (DOI: 10.1016/j.neurobiolaging.2010.07.018)
14. S.Hesketh, J.Sassoon, R.Knight, D.R.Brown, Elevated manganese levels in blood and CNS in human prion disease, Mol. Cell. Neurosci. 37 (2008) 590-598.
15. Y.Cheng, O.Zak, P.Aisen, S.C.Harrison, T.Walz, Structure of the Human Transferrin Receptor-Transferrin Complex, Cell, 116 (2004) 565-576.
16. H.Zhu, D.Alexeev, D.J.B.Hunter, D.J.Campopiano, P.J.Sadler, Oxo-iron clusters in a bacterial iron-trafficking protein: new roles for a conserved motif, Biochem. J. 376 (2003) 35-41.
17. F.Chiti, P.Webster, N.Taddei, A.Clark, M.Stefani, G.Ramponi, C.M.Dobson, Designing conditions for *in vitro* formation of amyloid protofilaments and fibrils, Proc. Natl. Acad. Sci. 96 (1999) 3590-3594.

18. R.A.Kyle, Amyloidosis a convoluted story. British J. Haematol, 114 (2001) 529-538.
19. M.B.Pepys, Amyloidosis. Ann. Rev. Med. 57 (2006) 223-241.
20. C.Ortiz, D.Zhang, A.E.Ribbe, Y.Xie, D.Ben-Amotz, Analysis of insulin amyloid fibrils by Raman spectroscopy, Biophy. Chem. 128 (2007) 150-155.
21. E.van der Linden, P.Venema, Self-assembly and aggregation of proteins, Curr. Opin. Coll. Int. Sc. 12 (2007) 158-165.
22. C.Wu, Z.Wang, H.Lei, W.Zhang, Y.Duan, Dual binding modes of Congo red to amyloid protofibril surface observed in molecular dynamics simulations, J. Am. Chem. Soc. 129 (2007) 1225-1232.
23. R.Wetzel, Ideas of order for amyloid fibril structure, Structure, 10 (2002) 1031-1036.
24. E.Žerovnik, Amyloid-fibril formation, Eur. J. Biochem. 269 (2002) 3362-3371.
25. M.R.Nilsson, C.M.Dobson, *In Vitro* Characterization of Lactoferrin Aggregation and Amyloid Formation, Biochem. 42 (2003) 375-382.
26. S.Ghosh, A.Mukherjee, P.J.Sadler, S.Verma, Periodic iron nanomineralization in human serum transferrin fibrils, Angew. Chem. Int. Ed. 47 (2008) 2217-2221.
27. W.W.Fish, Ferritin structure: possible models for apoferritin subunit arrangement, J. Theor. Biol. 60 (1976) 385-392.
28. E.C.Theil, Ferritin: structure, gene regulation, and cellular function in animals, plants, and microorganisms, Ann. Rev. Biochem. 56 (1987) 289-315.
29. J.Kwon, S.H.Park, C.Park, S.-O.Kwon, J.-S.Choi, Analysis of Membrane Proteome by Data-dependent LC-MS/MS Combined with Data-independent LC-MS^{E} Technique, J. Anal. Sci. Tech. 1 (2010) 78-85.
30. W.J.Hervey IV, M.B.Stradler, G.B. Hurst, Comparison of digestion protocols for microgram quantities of enriched protein samples, J. Proteome Res. 6 (2008) 3054-3061.

31. I.Horcas, R.Fernandez, J.M.Gomez-Rodriguez, J.Colchero, J.Gomez-Herrero, A.M.Baro, WSXM: A software for scanning probe microscopy and a tool for nanotechnology, Rev. of Sci. Instrum. 78 (2007) 013705 1-8.
32. F.W.Karasek, Plasma chromatography, Anal. Chem. 46 (1974) 710A-720A.
33. K.Giles, S.D.Pringle, K.R.Worthington, D.Little, J.L.Goose, R.H.Bateman, Applications of a travelling wave-based radio-frequency-only stacked ring ion guide, Rapid Commun. Mass Spectrom. 18 (2004) 2401-2414.
34. C.S.Creaser, J.R.Griffiths, C.J.Bramwell, S.Noreen, C.A.Hill, C.L.P.Thomas, Ion mobility spectrometry: a review. Part 1. Structural analysis by mobility measurement, Analyst, 129 (2004) 984-994.
35. B.T.Ruotolo, K.Giles, I.Campuzano, A.M.Sandercock, R.H.Bateman, C.V.Robinson, Evidence for Macromolecular Protein Rings in the Absence of Bulk Water, Science, 310 (2005) 1658-1661.
36. K.Thalassinos, J.H.Scrivens, Applications of traveling wave ion mobility mass spectrometry. Practical Aspects of Trapped Ion Mass Spectrometry, ed. R.E.March, J.F.J.Todd, 5, 2009, CRC Press.
37. K.Thalassinos, M.Grabenauer, S.E.Slade, G.R.Hilton, M.T.Bowers, J.H.Scrivens, Characterization of phosphorylated peptides using traveling wave-based and drift cell ion mobility mass spectrometry. Anal. Chem. 81 (2009) 248-254.
38. J.L.Wildgoose, K.Giles, S.D.Pringle, S.J.Koeniger, R.G.Valentine, R.H.Bateman, A comparison of travelling wave and drift tube ion mobility separations, in Proc. 54th ASMS Conf., Mass Spectrom. Allied Topics. 2006. Seattle.
39. P.D.Jeffrey, M.C.Bewley, R.T.MacGillivray, A.B.Mason, R.C.Woodworth, E.N.Baker, Ligand-induced conformational change in transferrins: crystal structure of

the open form of the N-terminal half-molecule of human transferrin, Biochem. 37 (1998) 13978-13986.

40. R.T.MacGillivray, S.A.Moore, J.Chen, B.F.Anderson, H.Baker, Y.Luo, M.Bewley, C.A.Smith, M.E.Murphy, Y.Wang, A.B.Mason, R.C.Woodworth, G.D.Brayer, E.N.Baker, Two high-resolution crystal structures of the recombinant N-lobe of human transferrin reveal a structural change implicated in iron release, Biochem. 37 (1998) 7919-7928.
41. D.M.Czajkowsky, Z.Shao, Inhibition of protein adsorption to muscovite mica by monovalent cations, J. Microsc. 211 (2003) 1-7.
42. T.A.Betley, M.M.Banaszak Holl, B.G.Orr, D.R.Swanson, D.A.Tomalia, J.R.Baker, Jr., Tapping mode atomic force microscopy investigation of poly(amidoamine) dendrimers: effects of substrate and pH on dendrimer Ddformation, Langmuir 17 (2001) 2768-2773.
43. R.Leverence, A.B.Mason, I.A.Kaltashov, Noncanonical interactions between serum transferrin and transferrin receptor evaluated with electrospray ionization mass spectrometry, Proc. Natl. Acad. Sci. 107 (2010) 8123-8128.
44. R.C.Beavis, T.Chaudhary, B.T.Chait, α-Cyano-4-hydroxycinnamic acid as a matrix for matrix-assisted laser desporption mass spectrometry, Org. Mass Spect. 27 (1992) 156-158.
45. M.G.Yefimova, A.Sow, I.Fontaine, V. Guilleminot, N.Martinat, P.Crepieux, S.Canepa, M.-C. Maurel, S. Fouche´court, E.Reiter, O. Benzakour, F.Guillou, Dimeric Transferrin Inhibits Phagocytosis of Residual Bodies by Testicular Rat Sertoli Cells, Biol. Reprod. 78 (2008) 697-704.

46. L.Bonsdorff, H.Tölö, E.Lindeberg, T.Nyman, A.Harju, J.Parkkinen, Development of a pharmaceutical apotransferrin product for iron binding therapy, Biologicals 29 (2001) 27-37.
47. J.-M.Jung, G.Savin, M.Pouzot, C.Schmitt, R.Mezzenga, Structure of heat-induced β-lactoglobulin aggregates and their complexes with Sodium-dodecyl sulfate. Biomacromolec. 9 (2008) 2477–2486.
48. A.S.Cavallaro, D.Mahony, M.Commins, T.J.Mahony, N.Mitter, Endotoxin-free purification for the isolation of Bovine Viral Diarrhoea Virus E2 protein from insoluble inclusion body aggregates. Microb. cell fact. 10 (2011) 1-9.
49. D.Gumerov, I.A.Kaltashov, Dynamics of iron release from transferrin N-lobe studied by electrospray ionization mass spectrometry. Anal. Chem. 73 (2001) 2565-2570.
50. S.Srisailam, T.K.S. Kumar, D.Rajalingam, K.M.Kathir, H.-S.Sheu, F.-J.Jan, P.-C.Chao, C.Yu, Amyloid-like fibril formation in an all β-barrel protein, J. Biol. Chem. 278 (2003) 17701-17709.
51. B.A.Wallace, Conformational changes by synchrotron radiation circular dichroism spectroscopy, Nat. Struct. Biol. 7 (2000) 708-709.
52. N.J.Greenfield, Using circular dichroism spectra to estimate protein secondary structure, Nat. Protoc. 1 (2006) 2876-2890.
53. A.J.Miles, B.A.Wallace, Synchrotron radiation circular dichroism spectroscopy of proteins and applications in structural and functional genomics, Chem. Soc. Rev. 35 (2006) 39-51.
54. W.E.Klunk, J.W.Pettegrew, D.J.Abraham, Quantitative Evaluation of Congo Red Binding to Amyloid-like Proteins with a Beta-pleated Sheet Conformation, J. Histochem.Soc. 37 (1989) 1273-1281.

55. C.Wu, Z.Wang, H.Lei, W.Zhang, Y.Duan, Dual binding modes of Congo red to amyloid protofibril surface observed in molecular dynamics simulations, J. Am. Chem. Soc. 129 (2007) 1225-1232.
56. H.Levine III, Thioflavine T interaction with synthetic Alzheimer's disease β-amyloid peptides: Detection of amyloid aggregation in solution. Prot. Sci. 2 (1993) 404-410.
57. W.E.Klunk, Y.Wang, G.-F.Huang, M.L.Debnath, D.P.Holt, C.A. Mathis, Uncharged thioflavin-T derivatives bind to amyloid-beta protein with high affinity and readily enter the brain, Life Sci. 69 (2001) 1471-1484.
58. R.Khurana, V.N.Uversky, L.Nielsen, A. L.Fink, Is Congo Red an Amyloid-specific Dye?, J. Biol. Chem. 276 (2001) 22715-22721.

Figure captions

Fig. 1. X-ray crystal structure of human serum transferrin showing the N- and C- lobes and their domains, and approximate dimensions. Only the C-lobe contains bound iron. Electron density from the glycan chains in the C-lobe is unresolved. The co-ordinates of this unpublished low resolution structure were kindly provided by H.Zuccola. A similar non-glycosylated structure of *apo*-transferrin has been published by Wally *et. al.* [3]; the structure of diferric human serum transferrin is expected to be published shortly [4].

Fig. 2. Schematic illustrating the sequence coverage obtained by LC-MS^E analysis of Novozymes recombinant transferrin (86%) expressed in *Saccharomyces cerevisiae.* This sequence differs from that of human transferrin at four amino acids (highlighted in red). Peptides which were identified are highlighted with the following colour key: blue - tryptic peptide; light green - partial peptide; bright green - partial modified tryptic peptide; other - overlapping identification *e.g.* teal - tryptic peptide and modified tryptic peptide).

Fig. 3. Deconvoluted mass spectrum showing non-glycosylated rTf at 75 098 Da and Ser32-glycosylated recombinant transferrin species at 75 260 Da (± 2 Da).

Fig. 4. AFM image of a transferrin fibre formed on a cleaved muscovite mica surface by evaporation of a 1 µM *holo*-transferrin solution showing both straight and curved sections; horizontal scale bar corresponds to 1 µm, vertical colour scale 4 nm. Inset: High resolution AFM image of the background layer (horizontal scale bar: 200 nm).

Fig. 5. ESI-mass spectra of recombinant human *holo*-transferrin from gel permeation chromatography separations of monomeric (**A**) $[M+21H]^{21+}$ to $[M+17H]^{17+}$ and dimeric (**B**) $[M+30H]^{30+}$ to $[M+26H]^{26+}$ fractions.

Fig. 6. ESI-mass spectrum of recombinant human *holo*-transferrin. The charge state distributions observed represent monomeric transferrin (M) from *ca.* 3700 to 4900 m/z ($[M+20H]^{20+}$ to $[M+16H]^{16+}$), dimeric transferrin (D) ($[M+29H]^{29+}$ to $[M+ 23H]^{23+}$) observed from *ca.* 5100 to 6800 m/z and higher order aggregates, which may be trimers or tetramers (T) with greater than 6500 m/z.

Fig. 7. Transmission electron microscopy micrographs of the dimer fraction (confirmed by ESI-MS) from anion exchange and size exclusion purification of 1 µM recombinant human *holo*-transferrin in 1 mM ammonium bicarbonate solution, dried on formvar copper grids. The formation of rounded (perhaps spherical) subunits is apparent. A 1% uranyl acetate stain has been applied.

Fig. 8. Transmission electron microscopy micrographs of the dimer fraction (confirmed by ESI-MS) from anion exchange and size exclusion purification of 1 µM recombinant human *holo*-transferrin in 1 mM ammonium bicarbonate solution, dried on formvar copper grids showing transferrin fibrils. A 1% uranyl acetate stain was applied.

Fig. 9. Estimated collisional cross-sections for *apo*- and *holo*-recombinant transferrin species at varying charge states.

Fig. 10. Overlay of crystal structures for *apo*-transferrin N-lobe (PDB ID 1BTJ) and *holo*-transferrin N-lobe (PDB ID 1A8E), with MOBCAL rotationally-averaged collisional cross-section estimations.

Fig. 11. Synchrotron radiation-circular dichroism spectrum of recombinant human *holo*-transferrin monomer (dashed line) and dimer (solid line) fractions (confirmed by ESI-MS), from 176 – 256 nm.

Fig. 1.

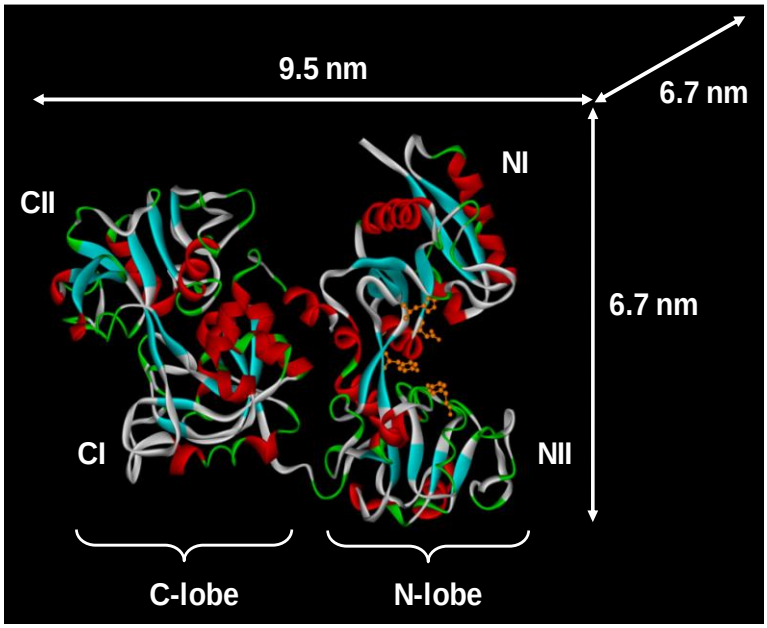

Fig. 2.


1 VPDKTVRWCA VSEHEATKCQ SFRDHMKSVI PSDGPSVACV KKASYLDCIR
51 AIAANEADAV TLDAGLVYDA YLAPNNLKPV VAEFYGSKED PQTFYYAVAV
101 VKKDSGFQMN QLRGKKSCHT GLGRSAGWNI PIGLLYCDLP EPRKPLEKAV
151 ANFFSGSCAP CADGTDFPQL CQLCPGCGCS TLNQYFGYSG AFKCLKDGAG
201 DVAFVKHSTI FENLANKADR DQYELLCLDN TRKPVDEYKD CHLAQVPSHT
251 VVARSMGGKE DLIWELLNQA QEHFGKDKSK EFQLFSSPHG KDLLFKDSAH
301 GFLKVPPRMD AKMYLGYEYV TAIRNLREGT CPEAPTDECK PVKWCALSHH
351 ERLKCDEWSV NSVGKIECVS AETTEDCIAK IMNGEADAMS LDGGFVYIAG
401 KCGLVPVLAE NYNKADNCED TPEAGYFAVA VVKKSASDLT WDNLKGKKSC
451 HTAVGRTAGW NIPMGLLYNK INHCRFDEFF SEGCAPGSKK DSSLCKLCMG
501 SGLNLCEPNN KEGYYGYTGA FRCLVEKGDV AFVKHQTVPQ NTGGKNPDPW
551 AKNLNEKDYE LLCLDGTRKP VEEYANCHLA RAPNHAVVTR KDKEACVHKI
601 LRQQQHLFGS DPADCSGNFC LFRSETKDLL FRDDTVCLAK LHDRNTYEKY
651 LGEEYVKAVG NLRKCSTSSL LEACTFRRP

Fig. 3.

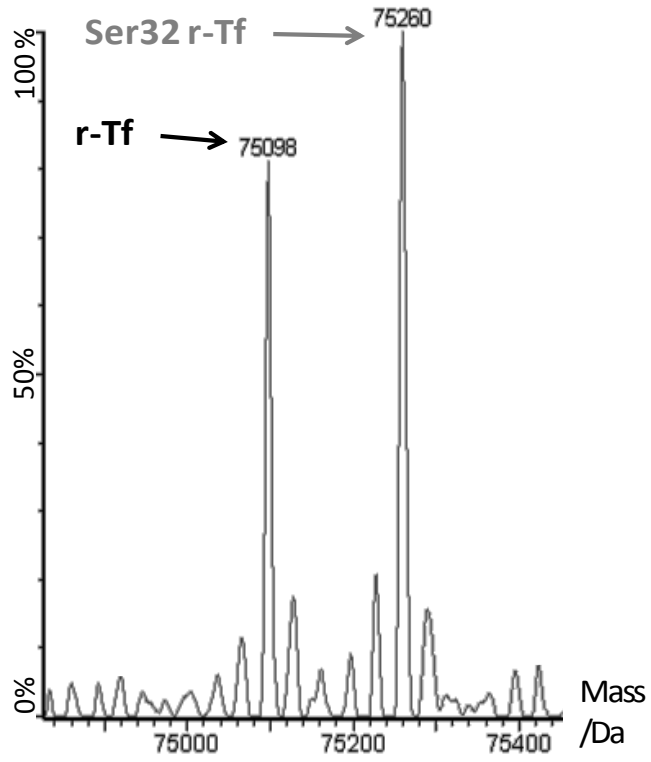

Fig. 4.

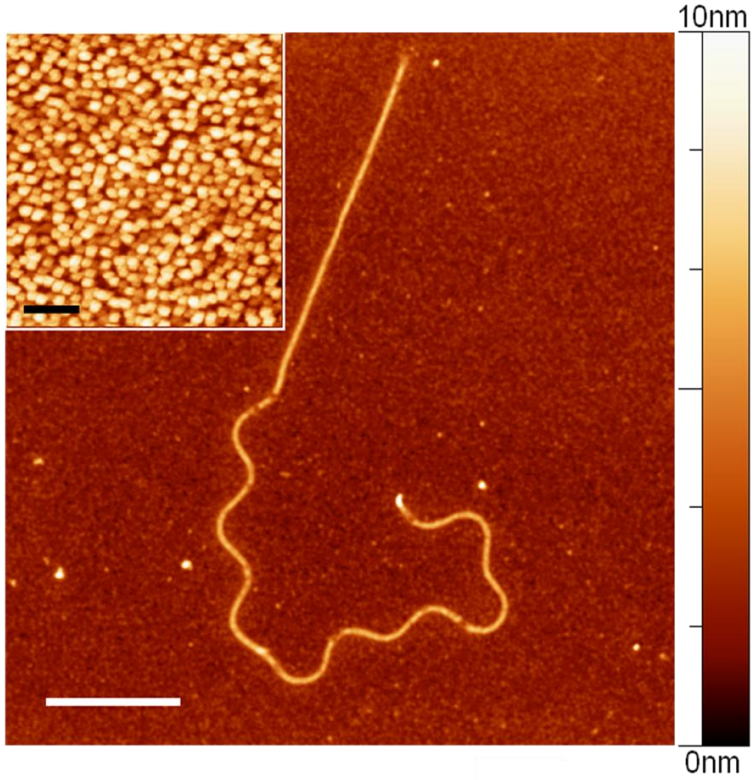

Fig. 5.

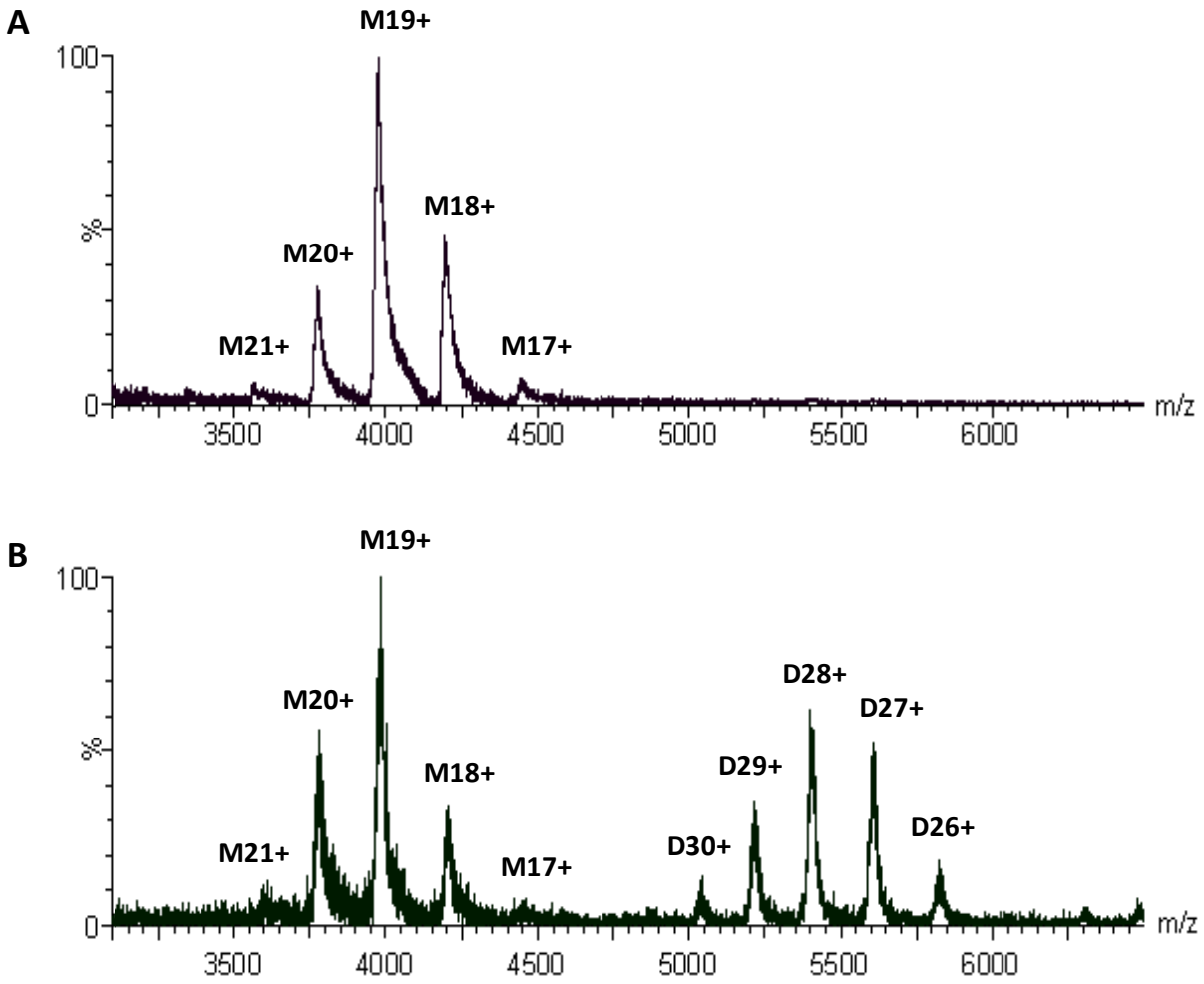
A
M19+
M18+
M20+
M21+
M17+
100
%
0
3500
4000
4500
5000
5500
6000
m/z
B
M19+
M20+
M18+
M21+
M17+
D28+
D27+
D29+
D26+
D30+
100
%
0
3500
4000
4500
5000
5500
6000
m/z

Fig. 6.

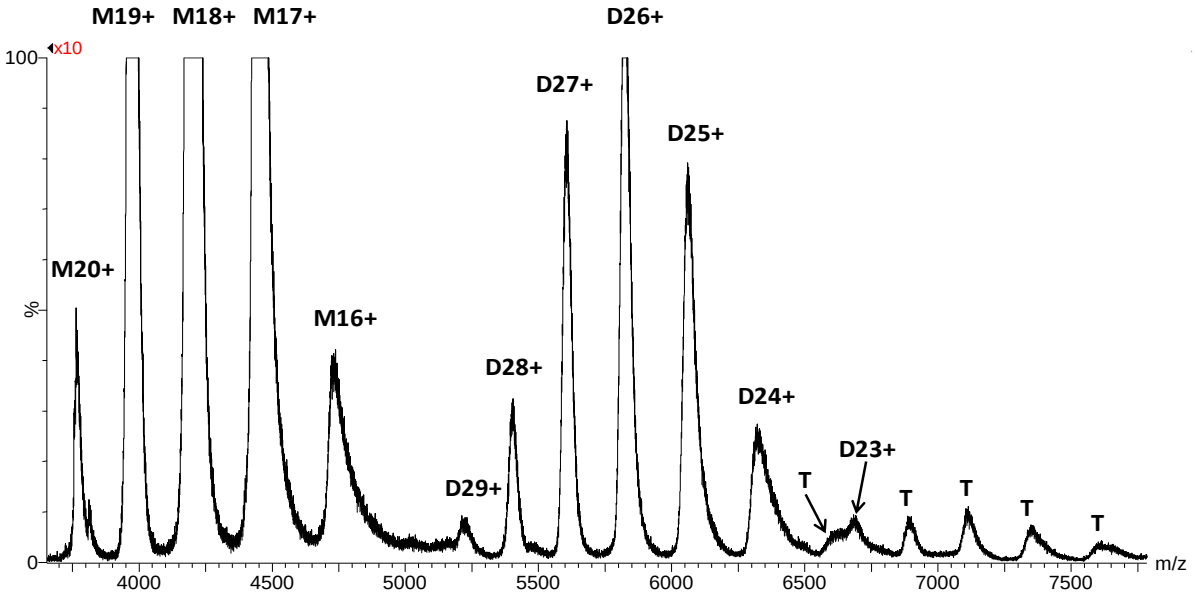
M19+
M18+
M17+
D26+
x10
100
D27+
D25+
M20+
M16+
%
D28+
D24+
D23+
T
D29+
T
T
T
T
0
4000
4500
5000
5500
6000
6500
7000
7500
m/z

Fig. 7.

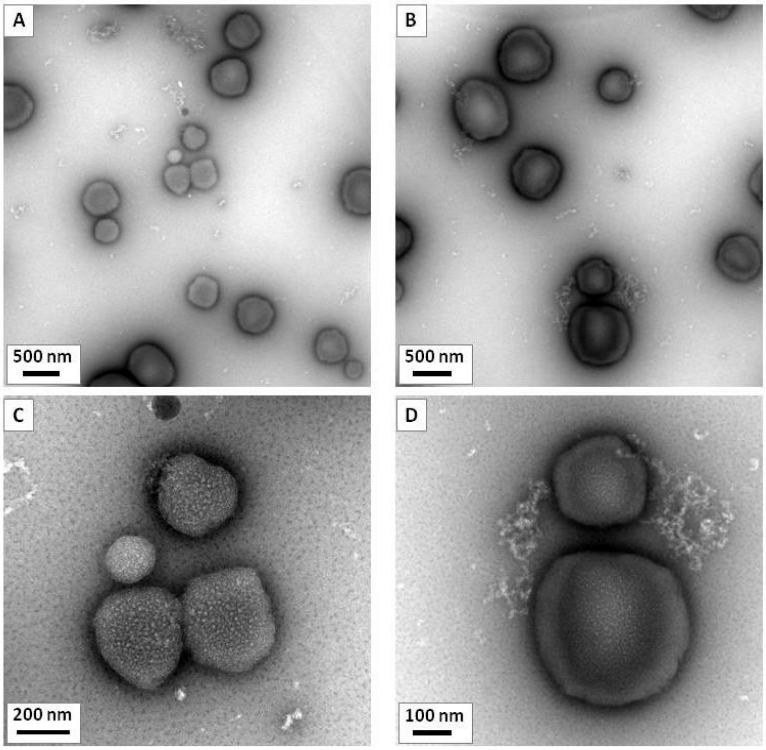

Fig. 8.

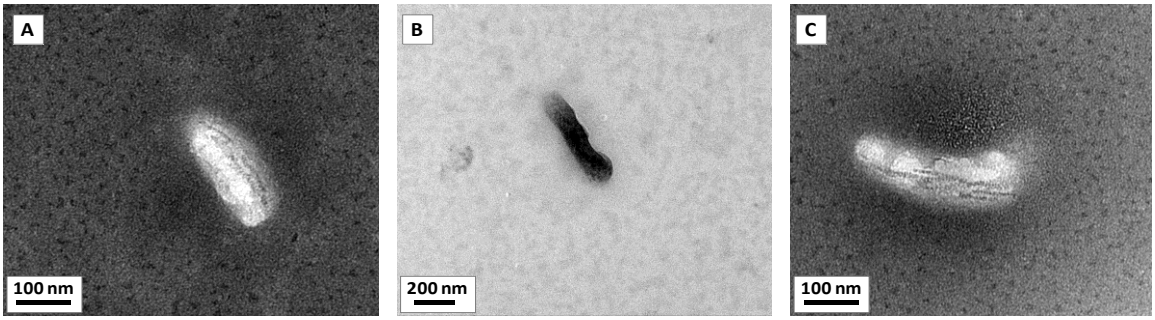

Fig. 9.

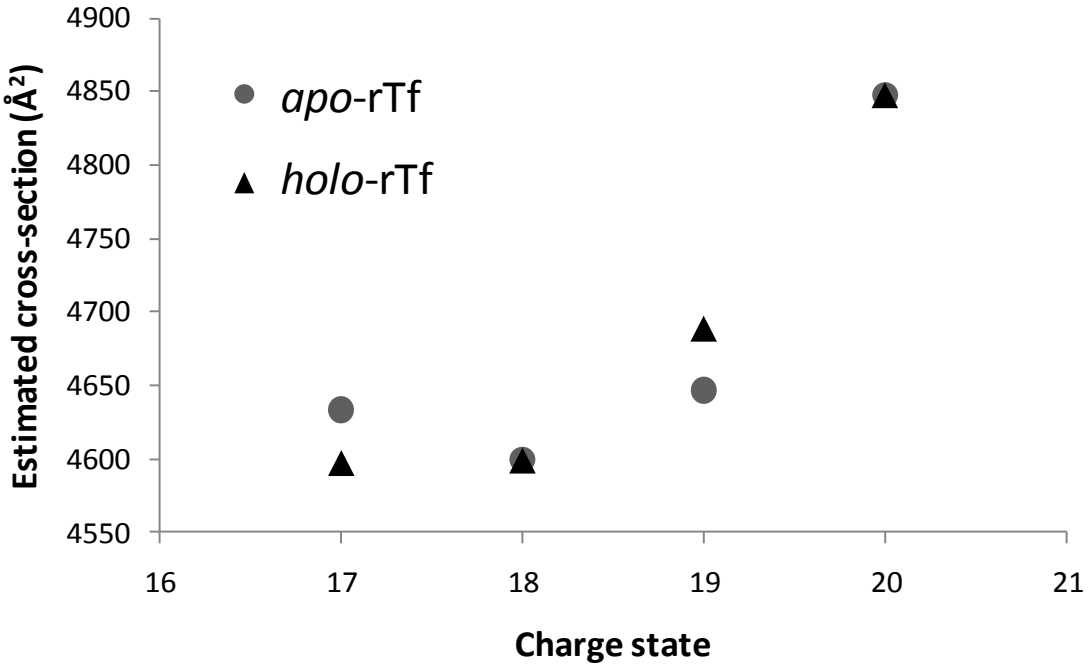
4900
4850
4800
4750
4700
4650
4600
4550
Estimated cross-section (Å²)
apo-rTf
holo-rTf
16
17
18
19
20
21
Charge state

Fig. 10.

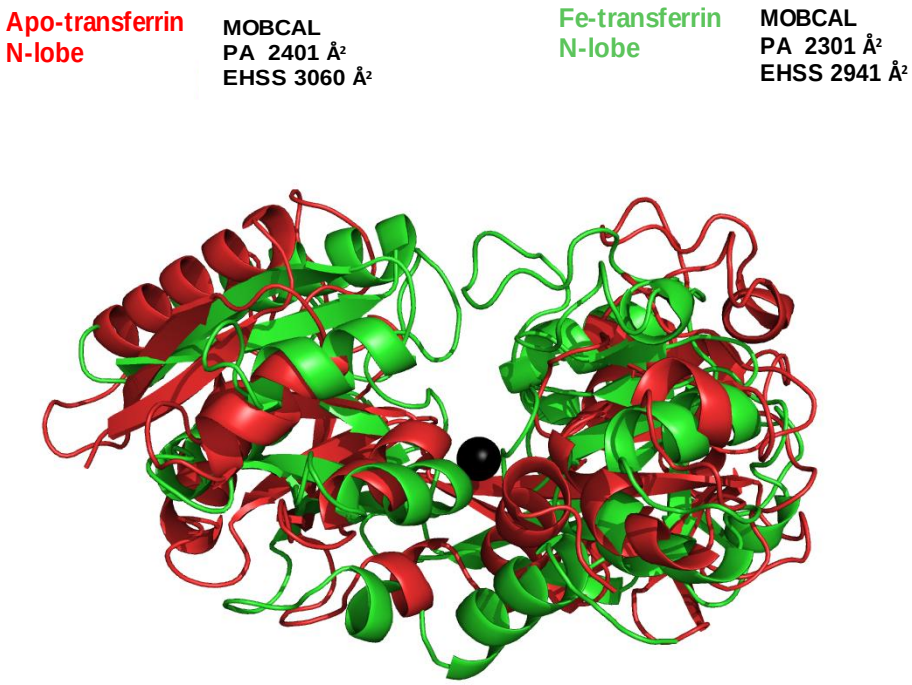
Apo-transferrin
N-lobe
MOBCAL
PA 2401 Å²
EHSS 3060 Å²
Fe-transferrin
N-lobe
MOBCAL
PA 2301 Å²
EHSS 2941 Å²

Fig. 11.

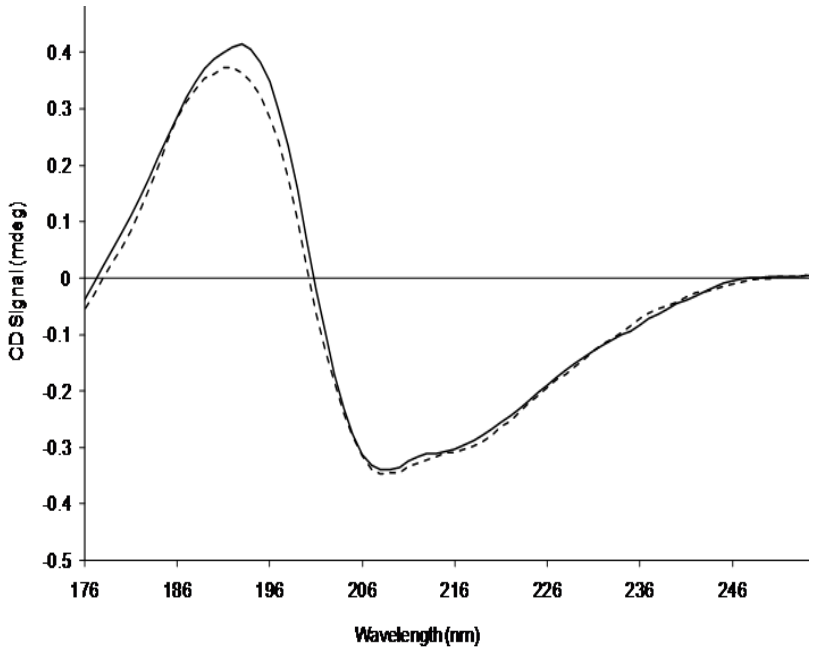
0.4
0.3
0.2
0.1
0
-0.1
-0.2
-0.3
-0.4
-0.5
CD Signal (mdeg)
176
186
196
206
216
226
236
246
Wavelength (nm)